

Comparative analysis and visualization of soil profiles at the meter spatial scale utilizing novel matrix and volume rendering techniques

Jake Gonzalez^{a,*}, Matthew Siebecker^b, Vung Pham^c, Cynthia Jordan^b, David C. Weindorf^d, Tommy Dang^a

^a Department of Computer Science, Texas Tech University, Lubbock, TX 79409, USA

^b Department of Plant and Soil Science, Texas Tech University, Lubbock, TX 79409, USA

^c Department of Computer Science, Sam Houston State University, Huntsville, TX 77341, USA

^d Department of Earth and Atmospheric Science, Central Michigan University, Mt. Pleasant, MI 48859, USA



ARTICLE INFO

Keywords:

Elemental concentration data
Data visualization and analytics
Portable X-ray fluorescence
NixPro proximal sensor
Alpha-shape scatter-plot matrix
Dimensionality reduction

ABSTRACT

This research introduces a soil characterization technique involving four data visualization tools to help researchers and stakeholders interpret high dimensional soil data at the field scale. This technique involves visualizing a reduced dimensionality representation of elemental concentration and color data gathered via portable X-ray fluorescence (pXRF) spectrometer and NixPro color proximal sensors, respectively. Soil cores were collected from sites located in Lubbock and Lamb Counties, West Texas, USA. Thirteen core samples were collected from these sites in a star pattern with readings from proximal sensors at depths ranging between 0 and 100 cm at 10 cm intervals. The dimensionality reduction techniques utilize four visualization tools to represent soil composition data through multiple user-adjustable variables (i.e., mg kg⁻¹ elemental concentrations and soil profiles), offering more insight and control compared to a single-variable approach. Through these tools and techniques, qualitative and quantitative conclusions regarding soil characteristics (e.g., elemental concentration variation, delineation of soil horizons, changes in soil color) can be formulated from the data and used in various applications. Areas where these novel software tools can be utilized potentially include rapid contaminant mapping in soils, characterization of diagnostic soil horizons (e.g., calcic, spodic, gypsic, etc.), micronutrient distribution at a field scale for precision agricultural purposes, and pedometrics.

1. Introduction

Portable X-ray fluorescence (pXRF) spectrometry is a proximal sensor technique which offers an economical way to accurately evaluate properties and features of soil samples in a rapid, easily portable, and non-invasive manner (Silva et al., 2021; Rouillon & Taylor, 2016; Lemiere, 2018). Complementary proximal sensor technologies, such as visible-near-infrared (vis-NIR) spectroscopy and the NixPro color sensor, are lowering the cost barrier of entry to precision farming and soil survey while offering a quick and robust avenue to acquire reliable data reflective of various soil properties (e.g., elemental concentration, organic carbon content, soil fertility, moisture retention, etc.) (Gozukara et al., 2021; Stiglitz et al., 2017; Xu et al., 2018). By utilizing these types of measurement devices on soil samples obtained through the “coring” method (Burridge et al., 2020; Wesson et al., 2014), elemental concentrations, certain mineralogical data, and soil diagnostic features

within the soil profile, and more broadly even within several hectares of a field site can be derived (Pham et al., 2021; Jordan, 2022). Such data collection techniques are becoming necessary for high priority soil analysis, throughput, and management (e.g., to assess and reduce risks of heavy metals in crops, monitor pollutant plumes (Cao et al., 2021), or evaluate trace nutrients within agricultural fields). This is critical information because the accumulation of heavy metals in agricultural soil decreases uptake of beneficial nutrients by crops, leading to reduced yield in crop production (Xu et al., 2016). Also, the presence of heavy metals above the recommended limits in crops consumed by humans can lead to adverse health effects (Weindorf et al., 2013; McGladdery et al., 2018; Zhuang et al., 2009). The ability to analyze the composition of farmland soil offers a great opportunity of increased crop yield, profitability, and sustainability, and most importantly, food safety as highlighted by the United States Food and Drug Administration’s Closer to Zero initiative (U.S. FDA, 2023).

* Corresponding author.

E-mail address: jake.gonzalez@ttu.edu (J. Gonzalez).

In this study, a 3D representation was modeled using approximated intermediate values between sensor readings taken from three soil sites via interpolation. Likewise, color data collected from the same sample cores at the same increments using a NixPro color sensor offer red blue green (RGB) values reliably and accurately representing the soil's color (Mancini et al., 2020). The resulting approximate interpolated elemental concentration levels and soil colors can then be used to construct a 3D volume representation from the 125,000 approximated data-points (Calcagno et al., 2008). Finally, principal component analysis (PCA) can be applied for dimensionality reduction and multivariate visualization approaches (i.e., parallel coordinates, alpha-shape scatterplot matrix, and 3D volume rendering) to visualize the data (Mora et al., 2017; Gonzalez & Dang, 2021; Pham et al., 2020).

The objectives of this study are to: 1) apply a numerical analysis approach (i.e., interpolation) to offer a more detailed representation of field collected soil data, 2) develop a data analytics approach implementation to provide visual representation of the collected data, and 3) examine how multivariate viewing spaces impact data interpretation. We hypothesize that when extending the dimensionality representation of high-dimensional (i.e., elemental concentration) soil data, insights into soil properties will be elucidated which may otherwise be hidden in single dimension representations. Also, by offering a detailed 3D volume representation, fluctuation in elemental concentrations throughout sampled locations can be visualized. These data presentation methods aim to aid soil and environmental researchers in decision making and examination pertaining to soil characteristics, mineralogy, moisture content, organic matter content, and precise fertilizer application.

2. Materials and methods

Soil samples utilized for the implementation and evaluation of the four tools developed in this work were collected with assistance from the Soil Survey Staff of the United States Department of Agriculture (USDA) Natural Resources Conservation Service (NRCS) in Major Land Resource Area (MLRA) 77C: Southern High Plains – Southern Part. Thirteen soil cores were collected in a star pattern for each of the three soil sites. The designations for these sites are “L”, “S”, and “R”, which stand for Large Star, Small Star, and Rangeland soils, respectively. Soil cores from site L were collected with a horizontal and/or vertical separation of 200 m with an overall span of 800 m, while sites S and R featured a collection distance of 100 m and 400 m span. Fig. 1b features an overlay of the star pattern on a satellite image of site L. Notably, the number of sampling cores collected and distance between sampling core locations should reflect soil variability of the area, with deference to the factors of soil formation (Jenny, 2011), site specific management, and study objectives.

For higher resolution modeling, the vertical separation distance of collected cores can be reduced, or the number of sampling cores collected can be increased, as appropriate. Soil cores for profiles at sites L and S were taken from sites in northern Lubbock County, Texas adjacent to each other, and site R profile cores were taken from southern Lamb County, Texas. Site L featured a playa lake in its center, while the adjacent S profile was collected from exclusively upland areas; both sites are in actively farmed cropland. Site R was in native rangeland. Soils of the sampled areas include the Acuff (Fine-loamy, mixed, superactive, thermic Aridic Paleustolls), Estacado (Fine-loamy, mixed, superactive, thermic Aridic Paleustolls), Olton (Fine, mixed, superactive, thermic Aridic Paleustolls), Randall (Very-fine, smectitic, thermic Ustic Epiaquerts), and Lazbuddie (Fine, smectitic, thermic Calcic Haplusterts) soil series (Soil Survey Staff, 2023). Physicochemical properties of the soils studied herein are reported in the Soil Series Data Explorer (California Soil Resources Lab, 2023). The area generally features an ustic soil moisture regime and thermic soil temperature regime with a Köppen climate classification of BSk – cold semi-arid climate (Soil Survey Staff, 2023; Kottek et al., 2006). Additional information regarding sampling sites is offered by Pham et al. (2022) and Jordan (2022).

2.1. Data acquisition

All thirteen soil cores taken from each of the three sites via coring machinery integrated onto a flat-bed truck (Fig. 1a) were scanned at 10 cm intervals from zones of 0–10 cm to 90–100 cm with both an Olympus Vanta (Waltham, MA, USA) pXRF and a NixPro color sensor (Hamilton, Ontario, Canada). Fig. 1c depicts a demonstration of scanning extracted cores using a pXRF device; however, the data used in this study was collected in a laboratory setting. Samples were air-dried and ground to pass a 2 mm sieve prior to analysis. The pXRF spectrometer was calibrated using a 316 stainless steel calibration coin (Weindorf & Chakraborty, 2020). The instrument was operated at 10–50 keV in *Geochem Mode* with a dwell time of 120 s per beam with two separate beams (240 s for one total scan). National Institute of Standards and Technology (NIST) certified reference materials (2710a, 2711a) were used to confirm performance of the pXRF. Recovery percentage (%) was calculated as pXRF reported/NIST certified elemental content on an element-by-element basis per Koch et al. (2017). Recovery percentages (%) for the selected elements follow (NIST 2710a, 2711a): Al 93.6, 91.8; K 93.8, 84.8; Ca 79.7, 94.3; Ti 91.7, 91.8; Mn 90.7, 88.6; Fe 120.4, 121.2; Cu 109.7, 104.3; Zn 104.7, 103.9; Rb 98.6, 102.2; Pb 95.6, 99.3. See Jordan (2022) for additional methodology on soil preparation. Color data was gathered using a smartphone-based NixPro Color Sensor application (Nix Sensor Ltd.) paired with the NixPro color sensor via Bluetooth. The color sensor was used to collect three readings from

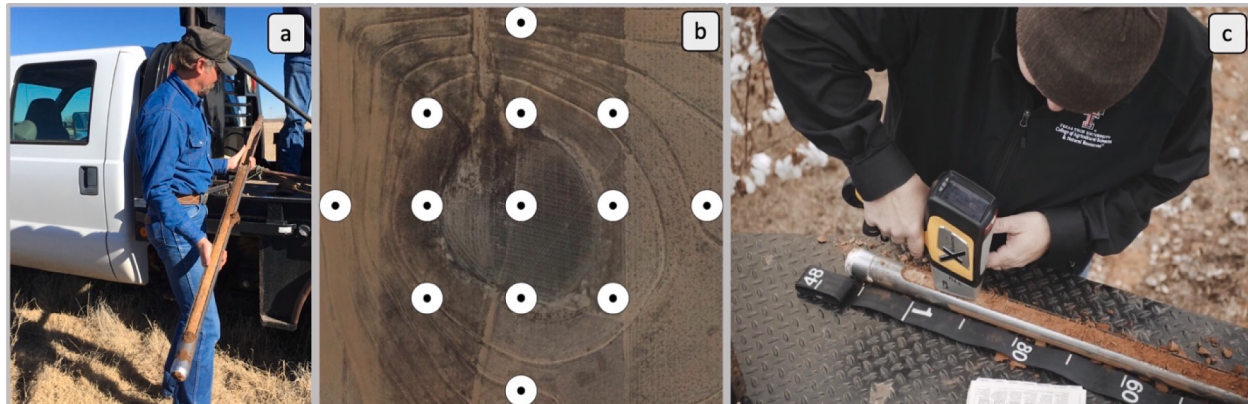


Fig. 1. Soil core extraction process, extraction pattern, and field sample scanning in Lubbock County, Texas, USA; (a) newly extracted soil core using machinery integrated onto a flat-bed truck; (b) star pattern collection locations of the thirteen cores overlaid on a satellite image of profile L; (c) demonstration of soil core elemental concentration data gathering via pXRF proximal sensor.

random locations within a small sample cup containing soil from the core interval zones. These three readings were averaged before recording RGB values to a spreadsheet.

The 13 georeferenced sample points per site (each containing a soil core of 1 m depth, separated by 10 cm intervals, yielding 130 data points per site) with appropriate elemental concentration and soil color data were used to generate interpolated data for a 3D volume rendering; this rendering was used to digitally reconstruct the soil profiles based on elemental abundance and soil color. For each of these data collection points, 36 unique elemental concentrations from the pXRF device were recorded alongside three RGB color values ranging from 0 to 255. Each of the data observations is represented using four methods, i.e., the four tools (1) PCA bi-plot, (2) 3D volume rendering, (3) alpha-shape scatterplot matrix, and (4) parallel coordinates chart. Fig. 2 demonstrates the data pipeline utilized in development of the presented data analytics technique involving: (a) data collection via proximal sensors, (b) sensor reading recording and interpolation, and (c) developed data visualization and soil analysis tools. Apart from elemental concentration and soil color data, three indices of pedological importance were also calculated: *Ruxton Weathering Index* (RI) defined as $\text{SiO}_2/\text{Al}_2\text{O}_3$, *Desilication Index* (DI) defined as $\text{SiO}_2/(\text{Al}_2\text{O}_3 + \text{Fe}_2\text{O}_3 + \text{TiO}_2)$, and *Elemental ratio of elements resistant to weathering*, also known as the *Stable Index* (SR) defined as Ti/Zr (Pham et al., 2022).

2.2. Data processing

To prepare the data for generating a 3D rendering of soil elemental concentrations, geostatistical interpolation via Kriging algorithm with a spatial model was undertaken for each of the 36 elemental concentration data variables, the three color data variables collected from the NixPro, and the three pedological indices calculated from the elemental concentration readings. The results from the interpolation step generated 125,000 approximated data points for each of the 42 data variables. These were used to construct a 3D volume representation of the sampled site. This interpolation approach is applied to provide a more refined overview of the sampled sites with greater detail without the cost and time implications accompanied with collecting a large number of samples needed to generate a similar result. For example, along the center lines of the star pattern sampled from the three sites, five cores were pulled for scanning with the pXRF device. These center lines have a length of 800 m for profile L and 400 m for profiles R and S. However, with Kriging interpolation applied to the readings, these five observation sites are effectively transformed into 50 observation locations along the same line of the original cores and extended the modeled radius of the sites by half of its respective sample collection separation on the XZ

plane. This approach is applied in all three spatial dimensions to generate the 125,000 approximated data observation locations from the 130 points (13 x 10) gathered at each site. Conversely, this interpolation technique introduces tradeoffs between collection separation distances and accuracy of interpolated values dependent upon inherent variability of the sampled sites.

2.3. Visualization methods

Each of the four visualization tools developed for the analysis process of this dataset provide a compressed representation of the high dimensional elemental concentration dataset collected from the soil sites. These representations facilitate overview characteristics recognition of a soil profile composition with regard to all 42 data variables or any subset thereof. Fig. 3 offers an overview to facilitate understanding of the four data analysis tools developed for the presented techniques and include (a) a PCA bi-plot, (b) 3D volume renderings, (c) an alpha-shape scatterplot matrix, and (d) a parallel coordinates chart.

To provide more flexibility, the variables are grouped into soil packages including Resource Conservation and Recovery Act (RCRA) 8 Metals, which are considered hazardous to human health and the environment (i.e., As, Ba, Cd, Cr, Pd, Hg, Se, and Ag), Plant Essential elements (i.e., Ca, Cu, Fe, K, Mn, S, and Zn), Pedology features used to classify and characterize soil properties (i.e., RI, DI, SR, and Rb), and Other (i.e., Mg, Al, Si, P, Ti, V, Co, Ni, Sr, Y, Zr, Nb, Mo, Sn, W, Bi, Th, U, Sb, and LE) (Environmental Protection Agency, 2023; [interactive Data Visualization Lab, 2023](#); Pham et al., 2022).

Segmenting elements in this way allows for the selection of individual elements or quickly choosing these groups of elements included in the visual analysis tool. Furthermore, either a single soil site can be selected to be represented, or any combination of the sites can be represented for comparison. Each of the four visualization methods takes a different approach for site comparison, which allows a user to derive conclusions about soil characteristics differing in nature (e.g., variations in elemental distribution or color). For example, imagine using such an approach to determine if a volume of soil across a landscape meets the base saturation and color requirements associated with a mollic epipedon (soil taxonomic classification). Each visualization in this analysis application is a web-based implementation using the JavaScript, HTML, and CSS languages along with portable library packages including Three.js and Data-Driven Document (D3) (Bostock et al., 2011). This allows a user to access and operate the application directly from a web browser and host the application from any web server. Furthermore, the underlying data powering the visualization could be structured and ported to variable-rate fertilizer applicators, however it is beyond the

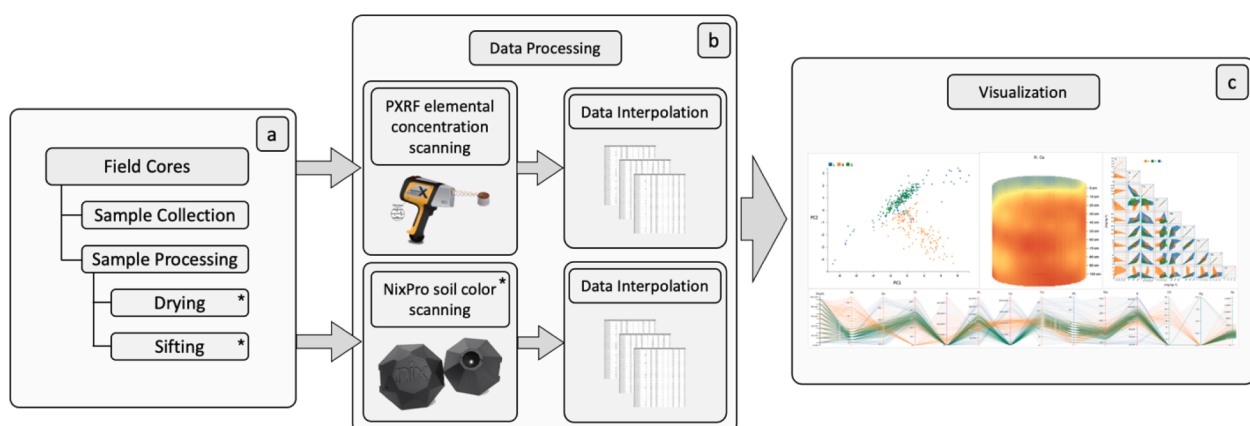


Fig. 2. Schematic of data pipeline used to characterize soil samples with the four data analytics techniques; (a) collection and processing of soil samples collected from the field; (b) elemental concentration readings gathered via portable X-ray fluorescence (pXRF) proximal sensor, and soil color data gathered via NixPro color sensor. Interpolation performed to process raw data for analysis tool ingestion; (c) reduced dimensional representations and visualizations of high dimensional soil data.

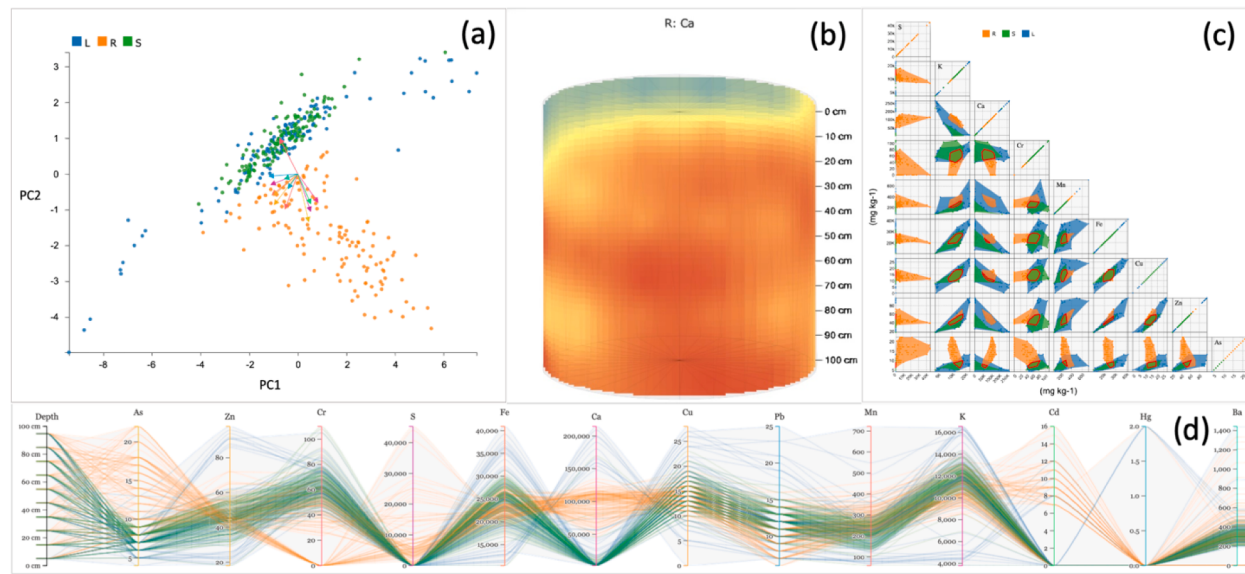


Fig. 3. Overview of the four tools developed to facilitate the proposed data analytics technique; (a) principal component analysis (PCA) dimensionality reduction bi-plot providing clustering and elemental correlation vectors; (b) 3D volume rendering using geostatic interpolated data; (c) an alpha-shape scatter-plot matrix with user adjustable alpha parameter and overlapping polygon area calculations; (d) parallel coordinates chart displaying multi-feature values for data observations. Shown soil data are collected in Lubbock and Lamb Counties, Texas, USA.

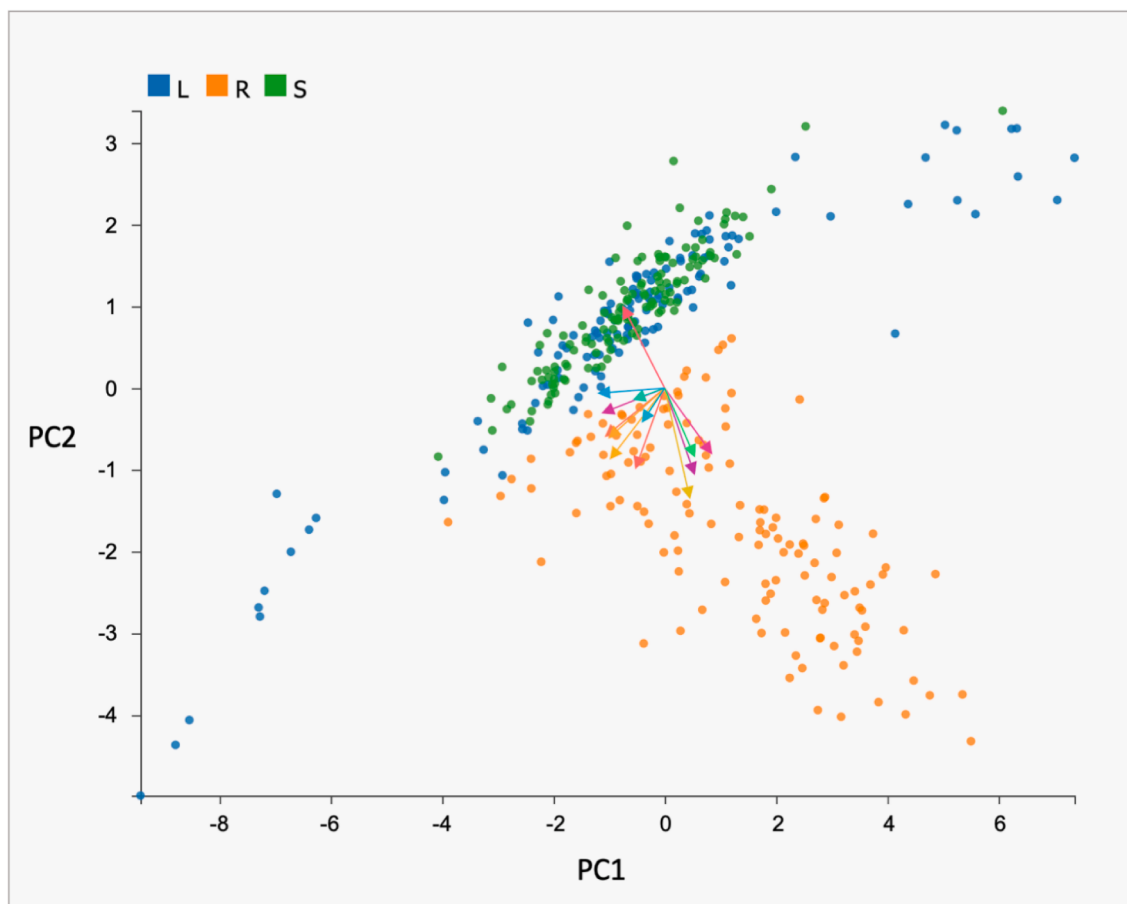


Fig. 4. Principal component analysis (PCA) dimensionality reduction bi-plot representing 36 dimensional data across soil profiles at sites L, R, and S with observation clustering and element contribution vectors. Shown soil data are collected in Lubbock and Lamb Counties, Texas, USA.

scope of this research.

3. Results

3.1. PCA bi-plot

PCA is an effective dimensionality reduction approach used to plot the high dimensional data obtained from the soils in a 2-dimensional plot where two calculated principal components are represented by the X and Y axis. These calculated components are linear combinations of the original variables that capture the largest amount of variation in the data, thus retaining the most important information about the data (Osinski et al., 2018). On the resulting bi-plot (Fig. 4), data sampled from different locations can form clusters depending on differing compositions of the sampled locations represented. Each dot on the bi-plot represents one of the 130 proximal sensor readings for a sample respective to all 36 elemental concentration variables, or a subset selected by a user. The color of each dot on the bi-plot signifies from which site the observation originates. Vectors are displayed on the origin of the bi-plot pointing in an independent direction to show each original variable's influence on the PCA result while its length represents the significance of influence. This provides valuable data to then input to other visualizations in the presented application. The main example of how resulting data from the PCA calculation interacts with other tools involves ordering of variables represented on the parallel coordinates chart, where a user can dissect the underlying data when analyzing an element's concentration influence. Each element vector is distinguishable based on its unique color which matches the color scheme on the parallel coordinates chart.

Furthermore, this PCA bi-plot has the capacity to show correlated variables. Elemental correlation can be identified by the angle between element variable vector representations on the bi-plot. Correlated elements will have an angular separation of < 90 degrees. If a pair of element vectors have an exact 90 degrees angular separation, the two elements have no correlation. Finally, if a pair of element vectors have an angular separation of > 90 and ≤ 180 degrees, the two elements are anticorrelated. This approach offers a quick visual representation of elemental concentration correlation across collective data from the soil profiles selected for analysis. Pedologically, this could be used for characterization of Fe/Mn concentrations, characterization of gypsum via Ca/S content, or characterization of spodic horizons via accumulations of Fe/Al. For demonstration, Fig. 5a highlights a finding that Pb and Zn are correlated based on the angular separation of the two element vector representations while soil profile L is selected for

Table 1

'L' sampled soil profile elemental pair Pearson correlation values. Shown soil data are collected in Lubbock and Lamb Counties, Texas, USA.

Rank	Element Pair	Pearson Correlation
1	Pb / Zn	0.947
2	Fe / Zn	0.924
3	Cu / Zn	0.896
:	:	:
64	Ca / Cu	-0.602
65	Ca / Fe	-0.635
66	Ca / K	-0.847

analysis, and Fig. 5b shows Ca and K are anticorrelated.

The association of elemental vectors can be compared with Table 1, where the three elemental concentration pairs with the greatest correlation along with the three pairs with the greatest anticorrelation determined via Pearson correlation evaluation of site L raw elemental concentration data are given. A user interaction is present on the PCA bi-plot allowing the user to hover the cursor over an element vector and the title of the appropriate variable (i.e., elemental symbol) is presented. This feature is to de-clutter the bi-plot of text during high level overview visualization of data while retaining the ability to offer more detailed information where deeper analysis is deemed appropriate. Similar hover features are also implemented on each data observation dot with a datapoint core location title along with a datapoint collection depth identifier. The color scheme of vector lines and arrows on the PCA bi-plot match the color scheme of vertical lines on the parallel coordinates chart with the same element matching in color. To combat outlier or anomalous data readings and prevent them from introducing noise into the visual representation of the dataset, an interaction was implemented to allow the removal of data points on the bi-plot. This can be done interactively in the Graphical User Interface by right clicking a mouse while hovering over an outlier data point. Doing so removes the data-point from the bi-plot and the remaining data points are used in a PCA recalculation. The ignored data points are added to a list on the side of the screen and can be re-added to the PCA visualization by clicking on the appropriate datapoint label.

3.2. 3D Volume rendering

3.2.1. Elemental distribution

As discussed in Section 2.2, the 130 data points collected with proximal sensors were interpolated resulting in 125,000 approximate values for each of the 36 elemental concentrations measured in

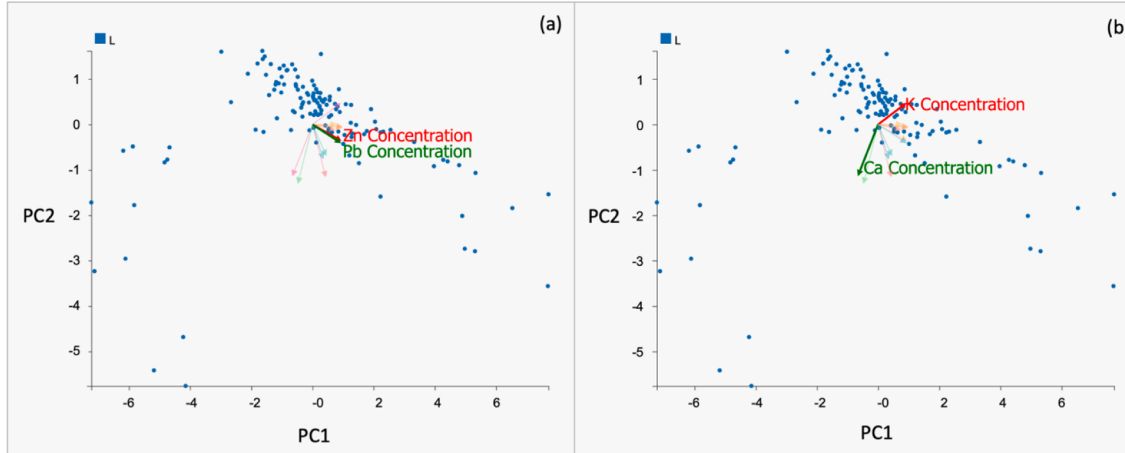


Fig. 5. Principal component analysis (PCA) dimensionality reduction bi-plot for profile L sampled soil site; **a**) correlated elemental concentrations signified by acute angle of separation between element vector (e.g., Zn and Pb); **b**) anticorrelated elemental concentrations signified by obtuse angles of separation between element vectors (e.g., K and Ca). Shown soil data are collected in Lubbock and Lamb Counties, Texas, USA.

milligrams per kilogram (mg kg^{-1}) with pXRF and for each of the three color variable readings from the NixPro sensor. To create a virtual representation of the soil cores and sample site, a color scale was used to signify the element concentration at a particular point within the sample. This is accomplished by normalizing the concentration data for a variable (scaling each data point to a range between 0 and 1 based on the minimum and maximum value i.e., $X_{\text{norm}} = (X - X_{\text{min}}) / (X_{\text{max}} - X_{\text{min}})$) and representing the low concentration end of the scale with a blue color and gradually traversing the color spectrum until reaching the color red, representing the maximum of the elemental concentration scale (Fig. 6).

The visualization has been implemented in a fashion allowing for the values to be re-scaled if multiple sites are selected to be rendered concurrently for the purpose of comparison (i.e., data from each profile is aggregated for creation of the normalized scale). This ensures a color scheme with the same concentration level across the selected profiles to match in color. As mentioned, this 3D volume rendering visualization is interactive via the parallel coordinates chart. The user is given the capacity to select an elemental concentration range on the chart to render only the sections of the 3D volume which satisfy the user-defined filtering criteria. This allows for the user to not just visualize an elemental concentration representation of the surface area of the cylinder but also visualize pockets within the cylinder with low, high, or any specified concentration level of a particular element. This would be a useful tool for contaminant mobility tracking, where a certain element threshold for human or environmental safety is of critical importance. For example, concerns often exist over subsoil pollutant migration or damage to agricultural lands following a chemical spill (e.g., Jha et al., 2021). This functionality is demonstrated in Fig. 7 where only sections within the 3D volume representation satisfying a filter of $> 100,000 \text{ mg kg}^{-1}$ Ca concentrations are rendered for both profiles R and L.

Furthermore, the user is not limited to one filtering parameter. The user can add filtering criteria for each of the elements deemed appropriate and displayed on the parallel coordinates chart. This visualization also allows direct user interaction involving rotating the 3D volume rendering along X, Y, and Z axes. A wireframe outlining the geometry of

the original site profile volume rendering provides visual reference when analyzing portions of the volume satisfying filtering criteria set on the parallel coordinates chart. A color scheme selector is available to the user allowing for elemental concentration visualization differing from element filtering criteria (i.e., rendering portions of the volume satisfying elemental concentration criteria, yet with a color scheme of a different elemental concentration). This feature also allows for other variables (i.e., actual soil color) to be visualized.

3.2.2. Visualizing soil color

The color scheme selector allows the user to select the real soil color scheme that renders the 3D volume using the interpolated RGB values collected using the NixPro color sensor. Because the color scheme can be decoupled from the selected elemental concentration filtering variable, a user can examine the soil color of locations within the sample sites satisfying filtering criteria. This is demonstrated in Fig. 8b where the same filtering criteria as Fig. 7 is applied. However, the soil color scheme is selected rather than elemental concentration color scheme. In this manner, soil color can also be spatially separated and pockets of color can be discerned. This extends the 2D color visualization provided by SoilWeb Apps (California Soil Resource Lab, 2023), allows for the inference of certain soil properties such as soil organic carbon content (Stiglitz et al., 2017), and corresponds to the classical soil color system (Munsell soil color) used for decades by the Soil Survey Staff in morphologically describing soils (Mancini et al., 2020; Swetha et al., 2022).

Graduation marks are also presented next to the volume for a depth reference, and a depth variable is incorporated onto the parallel coordinates chart allowing the user to select a portion of depth to render with interaction similar to selecting an element concentration range. Fig. 9 demonstrates how this filtering approach can be applied to examine the soil color of a cross-section of profiles R and L 50 cm below the surface. Because more than one variable can be selected for filtering, the depth variable can be coupled with other filtering criteria to examine cross-sectional cuts of soil profiles when elemental concentration

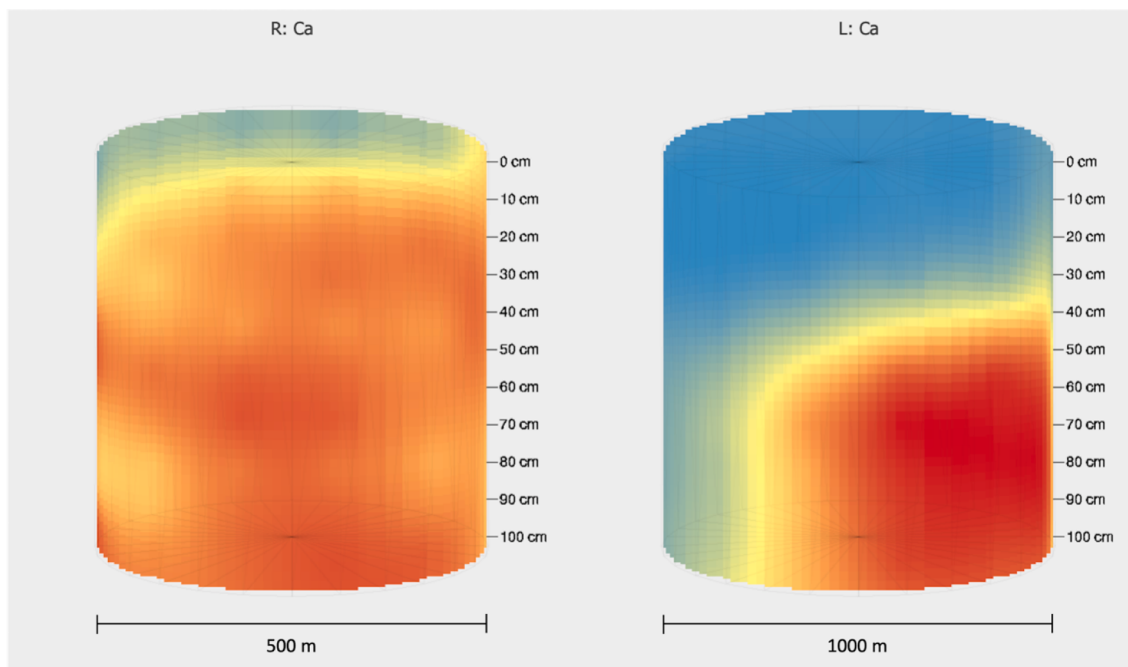


Fig. 6. 3D volume representation of site R and site L sampled soil profiles using 125,000 elemental concentration data points resulting from Kriging interpolation. The 3D plot can be manipulated by the user via mouse and graphical user interface (GUI) in this web-based software. The sites, each representing the 13 cores, are rendered with blue to red color spectrum. Low elemental concentration represented with a blue color and high elemental concentration represented with a red color. Shown soil data are collected in Lubbock and Lamb Counties, Texas, USA. (For interpretation of the references to color in this figure legend, the reader is referred to the web version of this article.)

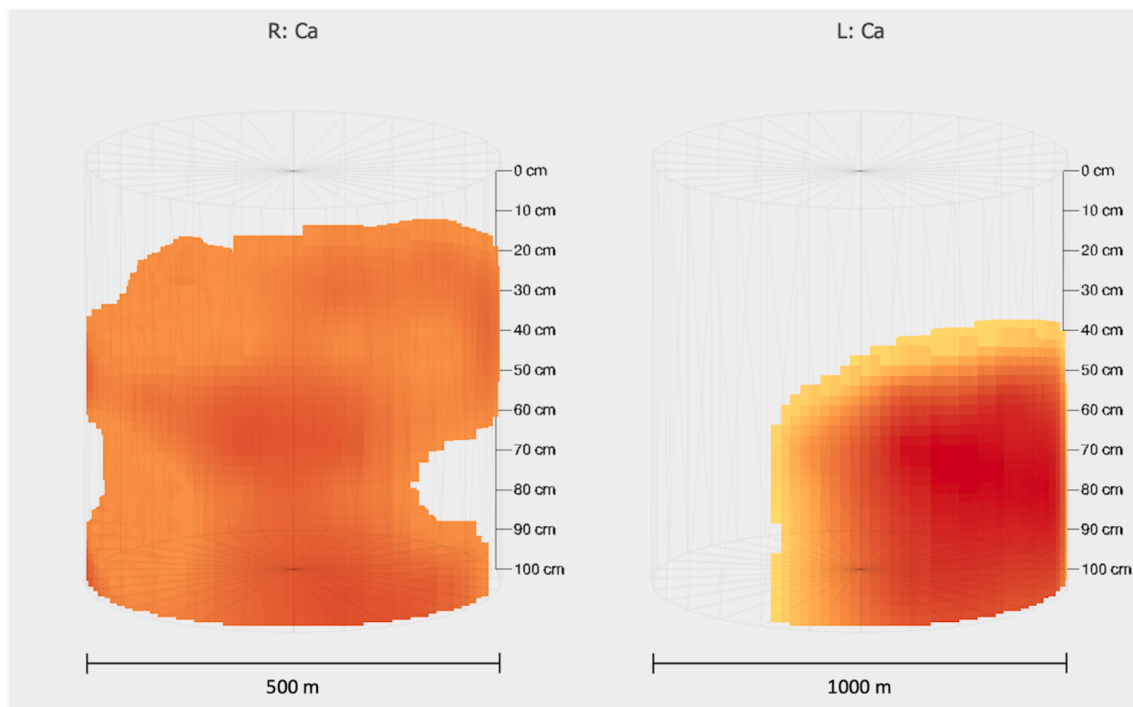


Fig. 7. 3D volume rendering of sampled soil profiles R and L with filtering criteria set on parallel coordinates chart for Ca concentration $> 100,000 \text{ mg kg}^{-1}$. Shown soil data are collected in Lubbock and Lamb Counties, Texas, USA.

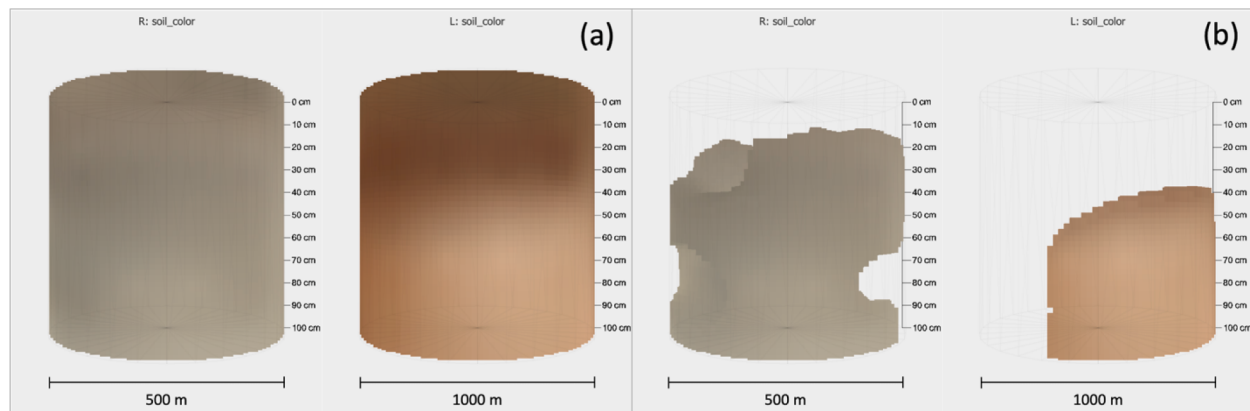


Fig. 8. 3D volume rendering with color scheme set to 'Soil Color'; (a) 3D volume rendering of profile R and L sampled soil sites; (b) profile R and L 3D rendering with filtering criteria of Ca concentration $> 100,000 \text{ mg kg}^{-1}$ applied. Shown soil data are collected in Lubbock and Lamb Counties, Texas, USA.

filtering is applied concurrently.

3.3. Alpha-shape scatter-plot matrix

Alpha-shape is a concept used in computational geometry to describe the shape of a set of points in Euclidean space. Alpha-shape overlays on a scatter-plot matrix aims to provide a pattern recognition tool among different pairs of variables in the dataset (Nguyen et al., 2020). For each pair of elements, alpha-shapes are calculated to determine if there is an overlapping portion for selected samples, which if present are outlined in a red line (Fig. 10). Information regarding the amount of overlapping area or separation distance between alpha-shapes can be used to examine which elemental combinations attribute to distinguishing characteristics of selected soil sites or which elemental combinations are similar. A slider option is available for adjusting a perimeter threshold of triangles connecting data points. These triangles result from Delaunay triangulation (Lee & Schachter, 1980), and their perimeter threshold is

known as the alpha parameter (Akkiraju et al., 1995). This alpha parameter has a range from 0 to 100 which coincides with the normalized minimum and maximum perimeter across selected soil profiles. As the alpha parameter approaches 0 the resulting alpha-shapes become more complex, while approaching 100 results in simpler alpha-shapes. An alpha parameter of 100 results in a convex hull which is the smallest convex polygon that contains the set of points. Finding an appropriate alpha parameter is dependent on the distribution of elemental concentration of selected pairs, however it is given that the overlapping area of alpha-shapes decreases as the alpha parameter decreased and vice versa. Also, lowering the alpha parameter can allow for the discovery of disjoint clustering within a soil profile. Fig. 10 depicts the alpha-shape matrix with the labels of each dimension located in the upper left of the subplots on the diagonal, and a view of a subplot with alpha-shape overlap. The X and Y axes on each subplot represent the mg kg^{-1} elemental concentration for the respective intersecting elements on the matrix. The effects of adjusting the alpha parameter is

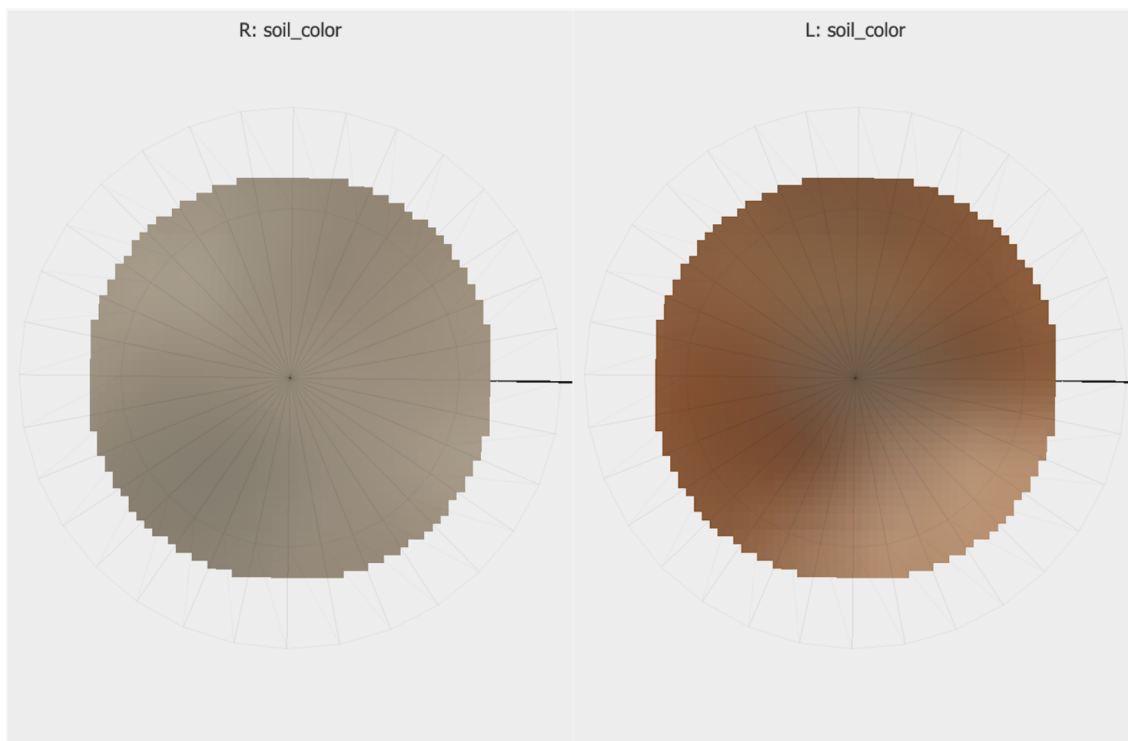


Fig. 9. 3D volume rendering of soil color at 50 cm depth for profile R and L sampled soil sites. Shown soil data are collected in Lubbock and Lamb Counties, Texas, USA.

later discussed and demonstrated in [Section 4](#).

Since the alpha parameter is a normalized value for each profile's Delaunay triangulation, each profile's polygon is affected with the same significance upon adjustment. Allowing the user to adjust the alpha parameter when evaluating soil samples is important since a discovery derived from one scatter-plot may differ from an alpha parameter leading to conclusions found from a differing scatter-plot. Furthermore, including variable pairs in the scatter-plot and Delaunay triangulation provides an avenue to potential insights when comparing samples which may not be easily recognizable using a single variable.

Since the alpha-shape polygons allow for the calculation of overlapping area, results indicating an absence of overlap are also noticeable. This is shown in [Fig. 10](#) where the lack of overlapping areas for sulfur is due to the lack or significantly low presence in two of the selected profiles. Thus, the formation of a one-dimensional line of datapoints dependent on the other element in the pair is caused instead of a two-dimensional polygon. A lack in alpha-shape overlap allows for a calculation of separation between selected samples. This is done by calculating the Euclidean distance using Pythagorean theorem separating each pair of observations between two samples to find the minimum distance of separation. The summation of these separations across a dimension can then be used to compare with the other selected variables to reorder the alpha-shape scatter-plot matrix with the most to least prominent starting at the left of the matrix. Reordering of the scatter-plot matrix can also be done with overlapping area totals and Pearson correlation values. With separations and overlapping area calculated for each of the subplots, filtering can be also achieved. This involves the user selecting an allowable range of the respective metric to highlight the subplots satisfying the criteria. [Fig. 11](#) demonstrates this filtering ability by highlighting scatter-plots which satisfies the correlation criteria set by three slider inputs. In this example, scatter-plots with elemental pairs with negative correlations on all three selected profiles are de-emphasized by lowering the opacity of the plot.

3.4. Parallel coordinates

Another approach to display high dimensional data sets to a user for comparison between data observations is via a parallel coordinates chart. This enables a user to directly compare elemental concentrations of individual data-points. [Fig. 12](#) shows how displaying each elemental dimension with a vertical line separated equidistant from the other variables allows the user to examine concentration recordings from one observation point across multiple variables (e.g., depth). Each data observation is represented as a path horizontally traversing and intersecting through each dimension's vertical line representation at a position relative to its value on the dimension scale. Each of these variables are scaled independently relative to the profiles selected for analysis, and the scaling can be reversed via a user interaction of clicking on a dimension label. A data path color signifies soil profile of represented data, while vertical lines have unique colors matching vector lines on the PCA bi-plot for the respective element. The ordering of these variables can also be altered with a click-and-drag interaction by the user in a scenario when observing two variables side-by-side would be more advantageous for certain investigations (e.g., to highlight different concentrations of two elements at separate depths in a core).

By connecting the four presented visualizations on a single application, interactions on one visualization can influence what is shown on another (i.e., data highlighting and filtering). [Section 3.1](#) discussed how the output of the PCA calculation influences the ordering of variables represented on the parallel coordinates chart with the most significant elemental concentration appearing to the left; however, this is not the only interaction between these two visualizations. Another interaction includes a lasso tool implemented on the PCA bi-plot allowing the user to draw a shape encapsulating data points for further investigation. When a subset of points is selected with the lasso tool, the data observations are highlighted on the parallel coordinates chart allowing for comparison with others in the dataset. Also, direct interaction on the parallel coordinates chart influences what is displayed on the 3D volume rendering of soil sites as discussed in [Section 3.2](#).

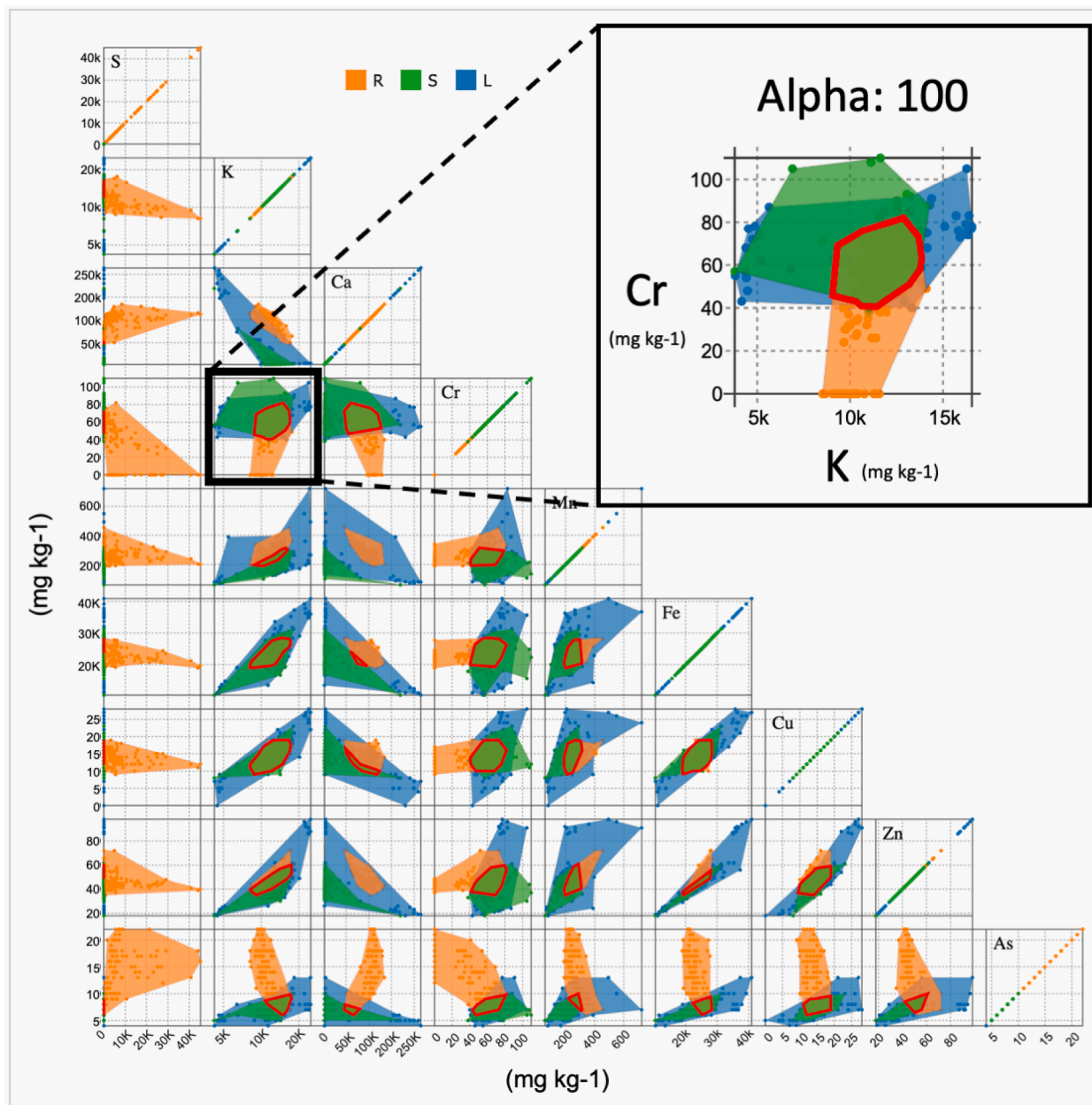


Fig. 10. Alpha-shape scatter-plot matrix with dimension labels positioned to the upper left of scatter-plots on the diagonal. Elemental pair scatter-plots located at vertical and horizontal intersections. The X and Y axes on each subplot represent mg kg^{-1} elemental concentration for the respective intersecting elements on the matrix. Alpha-shapes satisfying user input alpha parameter rendered, encapsulating appropriate datapoints on each subplot with same soil profile coloring scheme. Overlapping alpha-shape areas for selected profiles highlighted with a red perimeter. Shown soil data are collected in Lubbock and Lamb Counties, Texas, USA. (For interpretation of the references to color in this figure legend, the reader is referred to the web version of this article.)

4. Discussion

A notable advantage to visualizing the elemental concentrations in a scatter-plot matrix is to identify distinguishing patterns using two variables represented by independent dimensions. When analyzing the concentration data using only one dimension with these two elements, the user may be unable to identify distinguishing characteristics between the sampled profiles. This can be seen in the work by Singh et al. (2022) where a single variate analysis was used to detect heavy metal contamination, but such an approach is less suited for a field scale study to identify natural heterogeneity. Fig. 13a demonstrates where a separation is present between the alpha-shapes of R and S&L, which would not be easily uncovered using only one dimension. This is noted by the distribution density charts above and to the right of the scatter-plot

signifying the number of observations. To calculate these distribution densities, twenty equally sized bins were created and sequenced to span the dimension, with the total number of observations with elemental concentration readings falling within the range of a bin.

Fig. 9a demonstrates a large overlapping portion of the three sampled sites for K concentration; however, when dimensions K and Al are examined in tandem, a separation between profile observation clusters and alpha-shapes becomes apparent. This is resulting from the data samples having a similar correlation across the sampled soil sites; however, profile R has a more compact distribution in a range with a higher concentration of K. Fig. 13b also demonstrates similar findings for Ti and K concentrations. When examining each profile's distribution densities of Ti and K elemental concentrations, overlapping is present, yet the overlapping area created from alpha-shapes is minimal. When

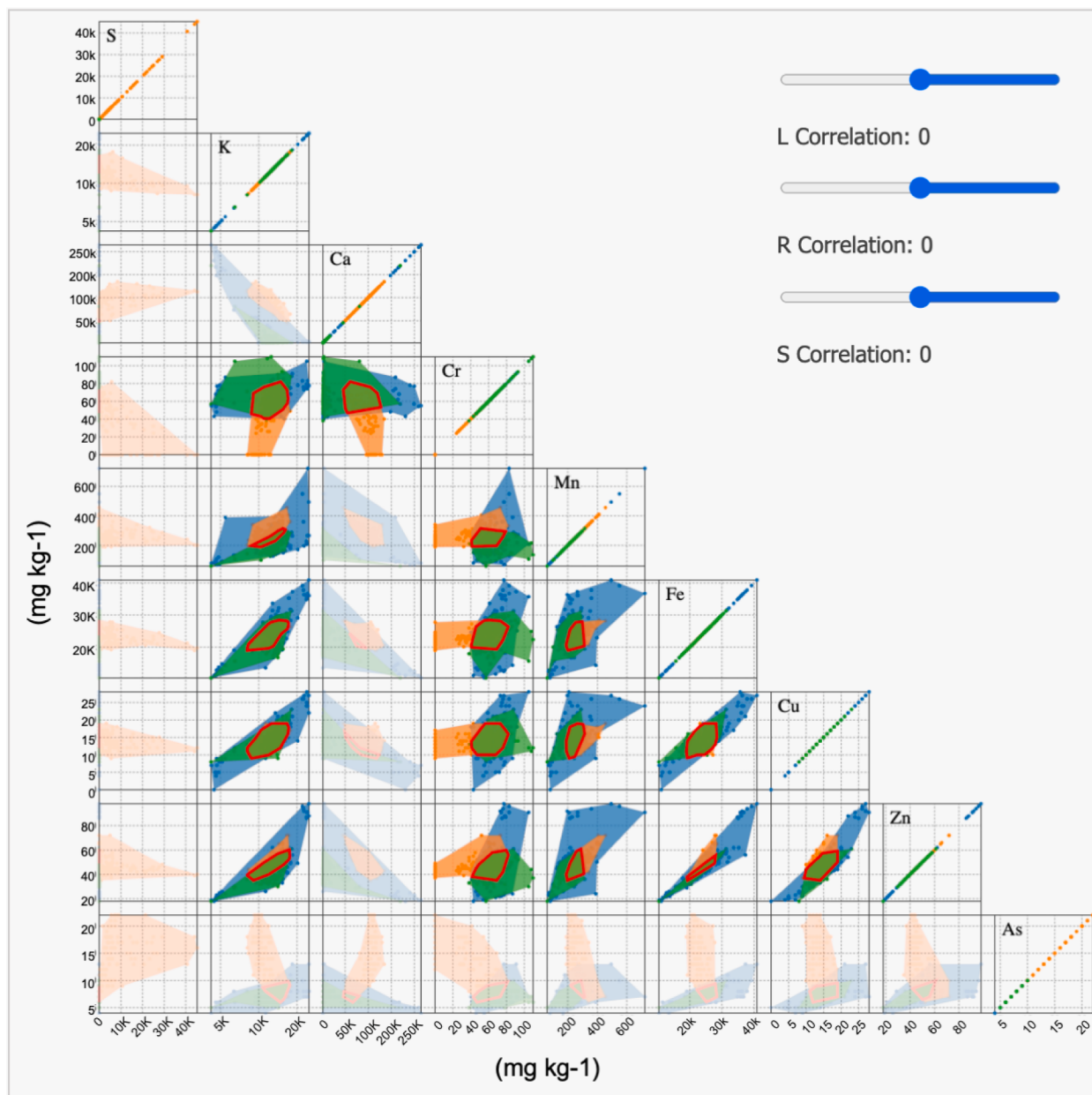


Fig. 11. Alpha-shape scatter-plot matrix with Pearson correlation filtering enabled to highlight sub-plots satisfying a non-negative correlation coefficient. Three sliders allow the user to independently control the desired correlation parameter for each selected soil profile. Shown soil data are collected in Lubbock and Lamb Counties, Texas, USA.

analyzing these element concentrations using two dimensions, the user can easily see the data distinguishing two of the sites because of a separation between the alpha-shapes of profiles R and S&L. Such findings would be less apparent using only a single dimension distribution density.

Fig. 14 highlights some of the insights which can be gained by changing the alpha parameter to create alpha-shape polygons around data points in the scatter plots. In both examples (Fig. 14), data observations for each of the sampled profiles fall into a distribution that is overlapping with that of the others. However, adjusting the alpha parameter allows the user control to uncover separation present in 2D space. Fig. 14a1 features an alpha parameter of 100 where the polygon encapsulating the R profile data observations fall within the alpha-shape of profile L. However, when the alpha parameter is changed to 40 (Fig. 14a2), separation between the observations becomes apparent in the 2D viewing space of elements Ca and Mn. Fig. 14b demonstrates

similar findings for Ca and Fe when comparing the alpha-shapes resulting from an alpha parameter of 100 and 60, also how the more complex alpha-shapes of a lower alpha parameter can remove overlapping portions on the scatter-plot. The examples present in Fig. 14 demonstrate how expanding the viewing space to multivariate relations leads to information which would otherwise remain hidden when viewing distribution densities in a single respective dimension separately. Both examples present in Fig. 14 show how varying alpha parameters can lead to independent findings for concentrations across different element pairs and how adjusting the alpha parameter is necessary when refining the visualization to denser distribution portions in the data of selected profiles.

The use of pXRF provides scientists and analysts a cost and time effective technique in acquiring numerous elemental concentration readings simultaneously, which can be utilized in even more applications than those highlighted above. Soil texture characterization and soil

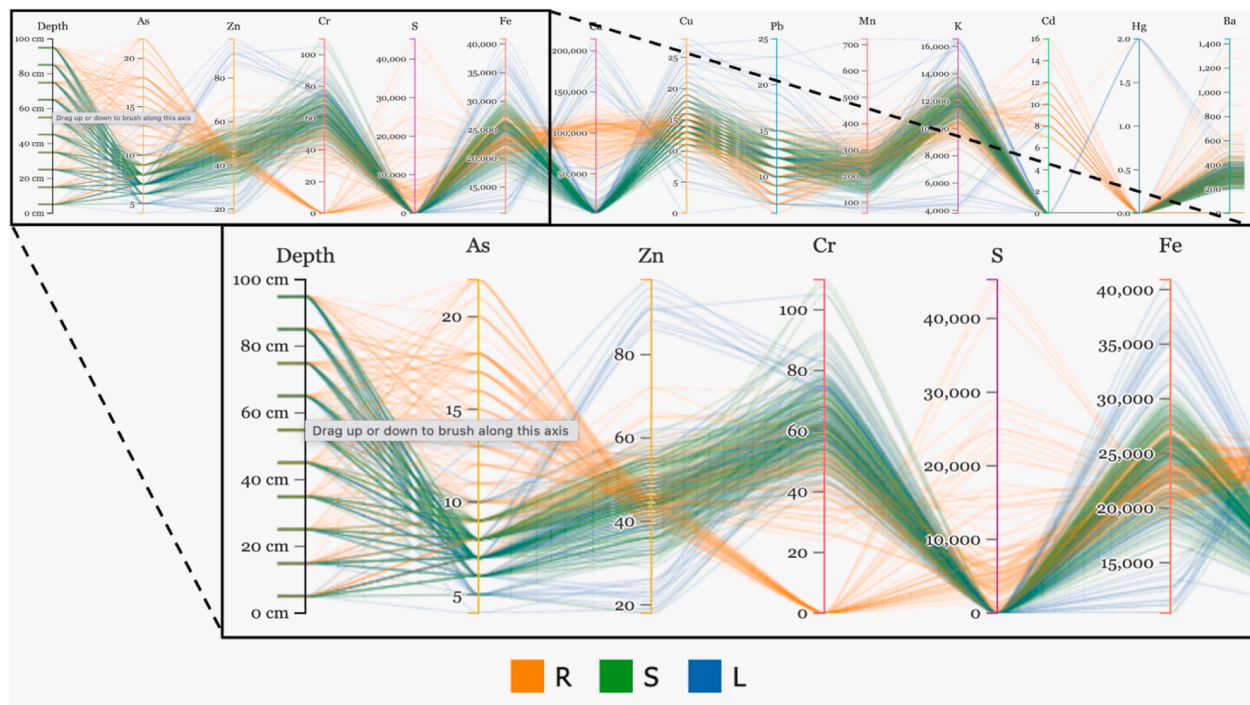


Fig. 12. Parallel coordinates chart representing each data observation as a path horizontally traversing and intersecting through each dimension's vertical line representation at a position relative to its value on the elemental concentration scale. Data path color signifies soil profile of represented data, while vertical lines have unique colors matching vector lines on principal component analysis (PCA) bi-plot. Shown soil data are collected in Lubbock and Lamb Counties, Texas, USA.

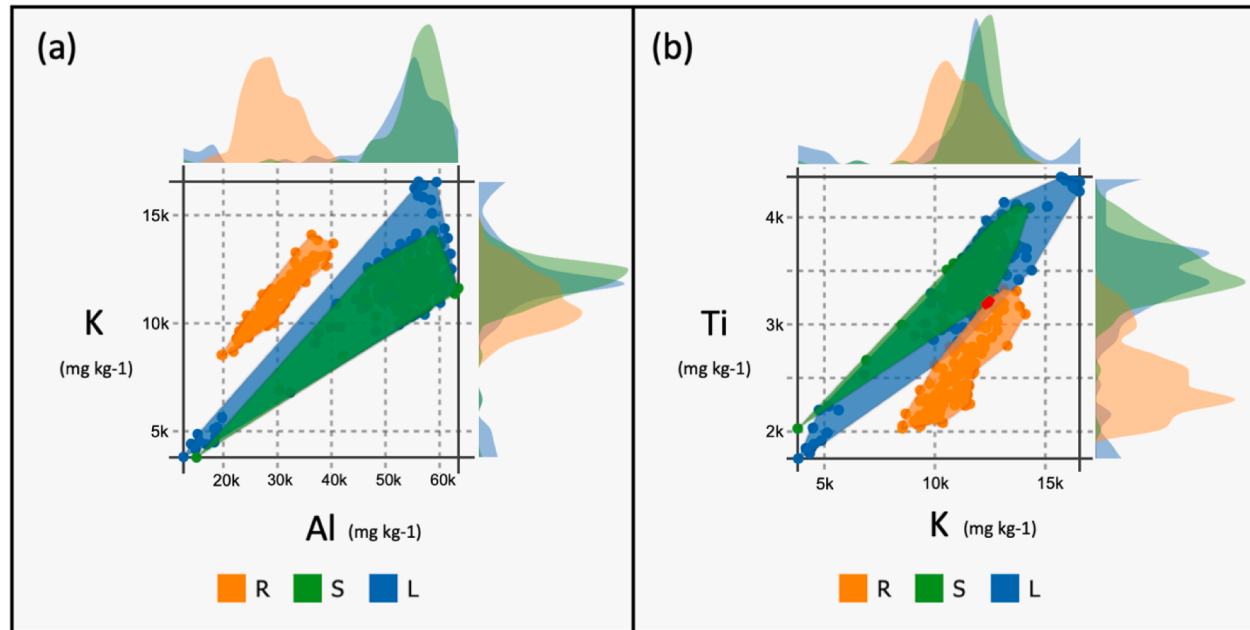


Fig. 13. Alpha-shape scatter-plots with profiles R, S, and L selected, highlighting advantage of a 2D viewing area. The X and Y axes represent mg kg^{-1} concentrations for respective elements with distribution densities overlaid on top and right of scatter-plot; (a) alpha-shape separation for K and Al when alpha is set to 100 along with distribution densities to the top and right of the scatter-plot; (b) Ti and K subplot with overlapping distribution densities for both dimensions yet minimal alpha-shape overlapping area. Shown soil data are collected in Lubbock and Lamb Counties, Texas, USA.

horizon differentiation (Zhu et al., 2011; Weindorf et al., 2012a) could also be inputted to the tool as discreet, field specific data for augmented visualization. With regard to soil texture characterization, one example scenario where alpha-shape visualization can be useful may involve the evaluation of soil texture where a scientist is using Fe and Rb concentrations as an indicator of clay content (Zhu et al., 2011). By displaying Fe and Rb within the alpha-shape scatter-plot matrix, the user would

have the ability to quickly evaluate differences or similarities in sampled soil horizons (depths). For example, some soil diagnostic horizons such as the argillic horizon can be differentiated based upon clay differences of as little as 3% in adjacent horizons, differences that can be challenging to identify in field settings (Soil Survey Staff, 2022).

Depending on the area covered during the data collection, variation could also quickly be uncovered via the clustering of datapoints on a

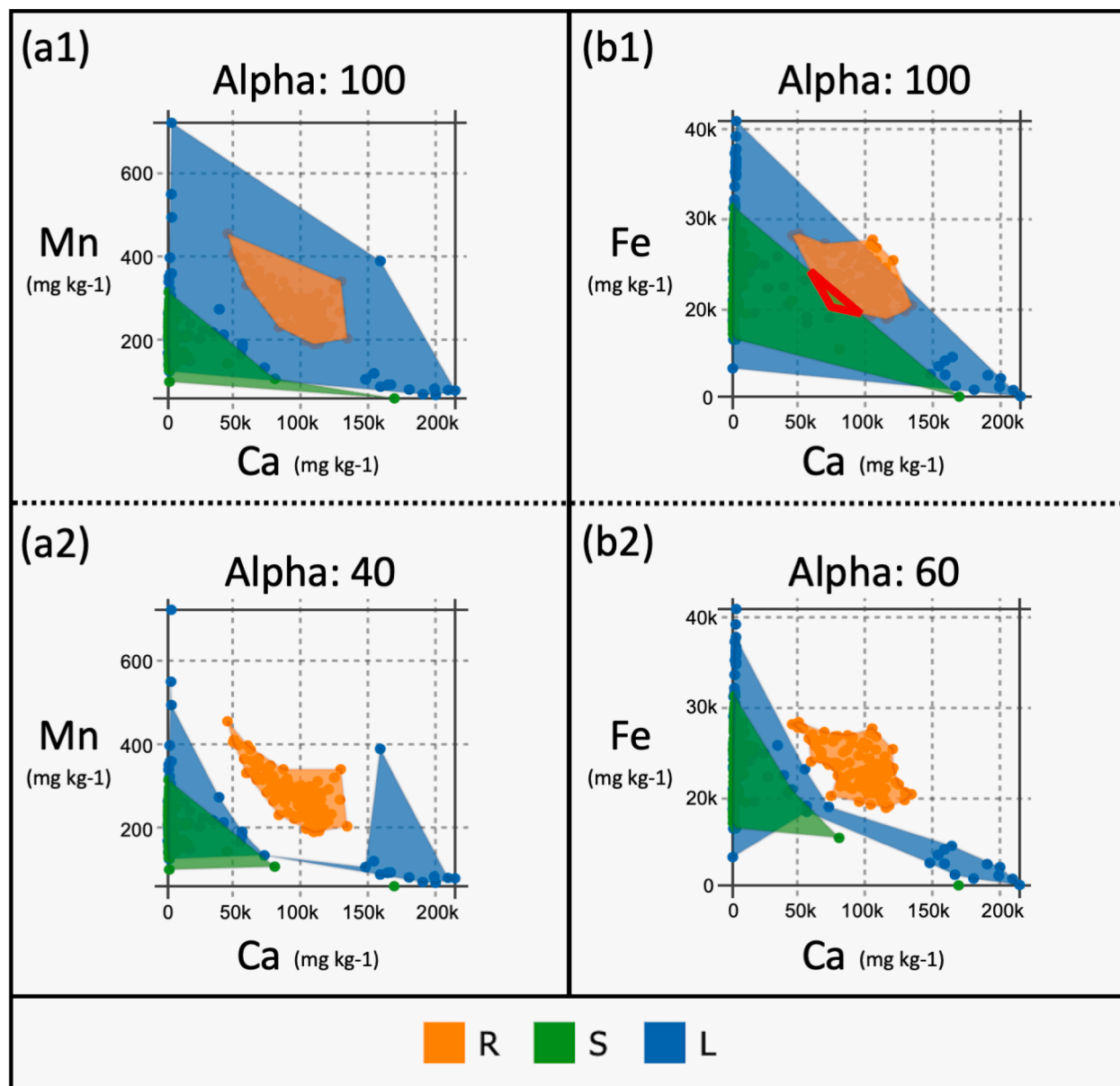


Fig. 14. Alpha-shape scatter-plot of three different elemental pairs signifying insights gained with varying alpha parameters with sites R, S, and L; (a) resulting alpha-shapes for Ca and Mn when alpha parameter changes from 100 to 40; (b) resulting alpha-shapes for Ca and Fe when alpha parameter changes from 100 to 60. Shown soil data are collected in Lubbock and Lamb Counties, Texas, USA.

plot. For soil horizon differentiation, the 3D volume rendering coupled with the Kriging interpolation offers a higher resolution visualization of how particular elemental concentrations (reflecting pedogenic properties) vary throughout a sampled soil site. For example, Weindorf et al., (2012b) used pXRF-derived elemental data to elucidate soil horizons in nondescript Ultisols and Inceptisols of Louisiana, USA. Similarly, Chakraborty et al. (2017) evaluated the pedogenic development of secondary carbonates using pXRF-derived Ca data in tandem with machine learning. Such elemental data can be optimally visualized in the tool while also taking advantage of filtering to render subregions and provide cross-sectional views at varying depths. Similarly, Sharma et al. (2015) used pXRF to predict soil cation exchange capacity (CEC), which commonly reflects soil nutrients/fertility. Spatially visualizing CEC can inform agronomists on where to make precision applications of fertilizer or other soil amendments for optimized crop production.

The advantages of the techniques shown herein notwithstanding, users must apply proper agronomic knowledge in translating the visualizations for real world results. For example, the visualization of

elements within the soil does not necessarily indicate that they are plant available as soil pH commonly influences elemental bioavailability. Similarly, soil color may indicate differences in soil organic matter content, but might also reflect differences in parent material derived from a lithologic discontinuity. For this reason, visualizations must be carefully considered with regard of all available information. Even so, from soil mapping and environmental quality assessment to agronomic evaluation and precision agriculture, the visualization techniques outlined herein provide new tools to help end users make better decisions in support of land stewardship and sustainability.

5. Conclusions

This research highlights the advantages of using an alpha-shape scatter-plot matrix as well as other dimensionality reduction data visualization techniques to draw insights from soil element compositional data and how such tools expedite conclusions relative to dissecting raw data. Each of the presented data visualizations offer different strengths.

The PCA bi-plot allows a user to see where soil site readings cluster on a reduced dimensional plot and offers vector representations on the bi-plot to further understand clustering and elemental concentration correlation. The parallel coordinates chart allows the user to directly compare data readings across sampled sites using raw collected data. The 3D volume rendering allows for visualizing elemental concentration variations spanning the sampled site and portions of the site satisfying filtering criteria (i.e., visualizing pockets of “hotspots” or variations in soil color). Finally, the alpha-shape scatter-plot matrix pairs variables to investigate compound concentration differences between sites as well as correlations and separations, which may otherwise be difficult to uncover using a single dimension. Aggregating each of these techniques to one application suite allows for interactions in one visualization tool to influence what is shown in another, advancing technique capabilities, enabling more flexibility for the user, and offering more complete overviews of soil profile and dataset characteristics. These novel software tools have potential uses including rapid contaminant mapping in soils, characterization of diagnostic soil horizons (e.g., calcic, spodic, gypsic, etc.), precision agriculture, and pedometrics.

Declaration of Competing Interest

The authors declare that they have no known competing financial interests or personal relationships that could have appeared to influence the work reported in this paper.

Data availability

Data will be made available on request.

Acknowledgements

In conducting this research, the authors gratefully acknowledge the contributions of the Lubbock Soil Survey Staff (Todd Carr, Alain Basurco, Craig Byrd, Kelly Attebury) and the BL Allen Endowment in Pedology at Texas Tech University.

References

- Akkiraju, N., Edelsbrunner, H., Facello, M., Fu, P., Mucke, E. P., Varela, C., 1995. Alpha shapes: definition and software. In: Proceedings of the 1st International Computational Geometry Software Workshop 63(66).
- Bostock, M., Ogievetsky, V., Heer, J., 2011. D³ Data-Driven Documents. IEEE Trans. Vis. Comput. Graph. 17 (12), 2301–2309. <https://doi.org/10.1109/TVCG.2011.185>.
- Burridge, J.D., Black, C.K., Nord, E.A., Postma, J.A., Sidhu, J.S., York, L.M., Lynch, J.P., 2020. An analysis of soil coring strategies to estimate root depth in maize (*Zea mays*) and common bean (*Phaseolus vulgaris*). Plant Phenomics 3252703. <https://doi.org/10.34133/2020/3252703>.
- Calcagno, P., Chilès, J.P., Courrioux, G., Guillen, A., 2008. Geological modelling from field data and geological knowledge; Part I. Modelling method coupling 3D potential-field interpolation and geological rules. Phys. Earth Planet. In. 171 (1–4), 147–157. <https://doi.org/10.1016/j.pepi.2008.06.013>.
- Cao, X., Gao, X., Zeng, X., Ma, Y., Gao, Y., Baeyens, W., Jia, Y., Liu, J., Wu, C., Su, S., 2021. Seeking for an optimal strategy to avoid arsenic and cadmium over-accumulation in crops: Soil management vs cultivar selection in a case study with maize. Chemosphere 272, 129891. <https://doi.org/10.1016/j.chemosphere.2021.129891>.
- Chakraborty, S., Weindorf, D.C., Weindorf, C.A., Das, B.S., Li, B., Duda, B., Pennington, S., Ortiz, R., 2017. Semi-quantitative evaluation of secondary carbonates via portable X-ray fluorescence spectrometry. Soil Sci. Soc. Am. J. 81, 844–852. <https://doi.org/10.2136/sssaj2017.01.0019>.
- Environmental Protection Agency, 2023. Available online at: <https://epa.gov> (verified 27 Mar. 2023).
- U.S. FDA, 2023. Closer to zero: Reducing childhood exposure to contaminants from foods. Available online at: <https://www.fda.gov/food/environmental-contaminants-food/closer-zero-reducing-childhood-exposure-contaminants-foods> (verified 27 Mar. 2023).
- Gonzalez, J., Dang, T., 2021. OutViz: Visualizing the outliers of multivariate time series. The 12th International Conference on Advances in Information Technology 37, 1–5. DOI:10.1145/3468784.3471606.
- Gozukara, G., Zhang, Y., Hartemink, A.E., 2021. Using vis-NIR and pXRF data to distinguish soil parent materials; an example using 136 pedons from Wisconsin, USA. Geoderma 396, 115091. <https://doi.org/10.1016/j.geoderma.2021.115091>.
- interactive Data Visualization Lab, 2023. Available online at: <https://idatavisualizationlab.github.io/> (verified 27 Mar. 2023).
- Jenny, H., 2011. Factors of soil formation: A system of quantitative pedology. Dover Publications, New York.
- Jha, G., Mukhopadhyay, S., Ulery, A.L., Lombard, K., Chakraborty, S., Weindorf, D.C., VanLeeuwen, D., Brungard, C., 2021. Agricultural soils of the Animas River watershed after the Gold King Mine spill: An elemental spatiotemporal analysis via portable X-ray fluorescence spectroscopy. J. Environ. Qual. 50 (3), 730–743. <https://doi.org/10.1002/jeq2.20209>.
- Jordan, C.M., 2022. Novel soil core visualization of diagnostic pedogenic feature. Master Thesis, Texas Tech University, Lubbock, TX. Available online at: <https://ttu-ir.tdl.org/bitstream/handle/2346/90029/JORDAN-THESIS-2022.pdf?sequence=1> (verified 27 Mar. 2023).
- Koch, J., Chakraborty, S., Li, B., Moore-Kucera, J., van Deventer, P., Daniell, A., Faul, C., Man, T., Pearson, D., Duda, B., Weindorf, C.A., Weindorf, D.C., 2017. Proximal sensor analysis of mine tailings in South Africa: An exploratory study. J. Geochem. Explor. 181, 45–57.
- Kottke, M., J. Grieser J., Beck, C., Rudolf, B., Rubel, F., 2006. World map of the Köppen-Geiger climate classification updated. Meteorologische Zeitschrift 15, 259–263. DOI: 10.1127/0941-2948/2006/0130.
- California Soil Resource Lab, 2023. SoilWeb Apps. Available online at: <https://casoilresource.lawr.ucdavis.edu/soilweb-apps/> (verified 27 Mar. 2023).
- Lee, D.T., Schachter, B.J., 1980. Two algorithms for constructing a Delaunay triangulation. Int. J. Comput. Inform. Sci. 9, 219–242. <https://doi.org/10.1007/BF00977785>.
- Lemiere, B., 2018. A review of pXRF (field portable X-ray fluorescence) applications for applied geochemistry. J. Geochem. Explor. 188, 350–363. <https://doi.org/10.1016/j.geexplo.2018.02.006>.
- Mancini, M., Weindorf, D.C., Monteiro, M.E.C., de Faria, Á.J.G., dos Santos Teixeira, A. F., de Lima, W., de Lima, F.R.D., Dijair, T.S.B., Marques, F.D., Ribeiro, D., Silva, S.H. G., Chakraborty, S., Curi, N., 2020. From sensor data to Munsell color system: Machine learning algorithm applied to tropical soil color classification via NiX™ Pro sensor. Geoderma 375, 114471. <https://doi.org/10.1016/j.geoderma.2020.114471>.
- McGladdery, C., Weindorf, D.C., Chakraborty, S., Li, B., Paulette, L., Podar, D., Pearson, D., Kusi, N.Y.O., Duda, B., 2018. Elemental assessment of vegetation via portable X-ray fluorescence (PXRF) spectrometry. J. Environ. Manage. 210, 210–225. <https://doi.org/10.1016/j.jenvman.2018.01.003>.
- Mora, J.L., Herrero, J., Weindorf, D.C., 2017. Multivariate analysis of soil salinization-desalinization in a semi-arid irrigated district of Spain. Geoderma 291, 1–10. <https://doi.org/10.1016/j.geoderma.2016.12.018>.
- Nguyen, Q.V., Miller, N., Arness, D., Huang, W., Huang, M.L., Simoff, S., 2020. Evaluation on interactive visualization data with scatterplots. Visual Informatics 4 (4), 1–10. <https://doi.org/10.1016/j.visinf.2020.09.004>.
- Osinski, G., Osinska, V., Malak, P., 2018. PCA algorithms in the visualization of big data from polish digital libraries. Advances in Intelligent Systems and Computing 833, 522–532. https://doi.org/10.1007/978-3-319-98678-4_52.
- Pham, V., Weindorf, D., Dang, T., 2020. SoilScanner: 3D Visualization for soil profiling using portable X-ray fluorescence. Workshop on Visualisation in Environmental Sciences (EnvVis). <https://doi.org/10.2312/envvis.20201094>.
- Pham, V., Weindorf, D.C., Dang, T., 2021. Soil profile analysis using interactive visualizations, machine learning, and deep learning. Comput. Electron. Agric. 191, 106539 <https://doi.org/10.1016/j.compag.2021.106539>.
- Pham, V., Jordan, C.M., Siebecker, M.G., Weindorf, D.C., Dang, T., 2022. iDVS: interactive 2D and 3D visualizations of proximal sensor data for rapid characterization of soil profiles. Precis. Agric. <https://doi.org/10.1007/s11119-022-0996-8>.
- Rouillon, M., Taylor, M.P., 2016. Can field portable X-ray fluorescence (pXRF) produce high quality data for application in environmental contamination research? Environ. Pollut. 214, 255–264. <https://doi.org/10.1016/j.envpol.2016.03.055>.
- Sharma, A., Weindorf, D.C., Wang, D.D., Chakraborty, S., 2015. Characterizing soils via portable X-ray fluorescence spectrometer: 4. Cation exchange capacity (CEC). Geoderma 239–240, 130–134. <https://doi.org/10.1016/j.geoderma.2014.10.001>.
- Silva, S.H.G., Ribeiro, B.T., Guerra, M.B.B., de Carvalho, H.W.P., Lopes, G., Carvalho, G. S., Guilherme, L.R.G., Resende, M., Mancini, M., Curi, N., Rafael, R.B.A., Cardelli, V., Cocco, S., Corti, G., Chakraborty, S., Li, B., Weindorf, D.C., 2021. PXRF in tropical soils: Methodology, applications, achievements and challenges. Adv. Agron. 167 <https://doi.org/10.1016/bs.agron.2020.12.001>.
- Singh, P., Datta, M., Rama, G., Gupta, S., Malik, T., 2022. Qualitative comparison of elemental concentration in soils and other geomaterials using FP-XRF. PLoS One 17, 5. <https://doi.org/10.1371/journal.pone.0268268>.
- Soil Survey Staff, 2022. Keys to Soil Taxonomy, 13th ed. USDA-Natural Resources Conservation Service. Available online at: <https://www.nrcs.usda.gov/resources/guides-and-instructions/keys-to-soil-taxonomy#keys> (verified 27 Mar. 2023).
- Soil Survey Staff, 2023. Web soil survey. Available online at: <https://websoilsurvey.sc.egov.usda.gov/App/HomePage.htm> (verified 27 Mar. 2023).
- Stiglitz, R., Mikailova, E., Post, C., Schlautman, M., Sharp, J., 2017. Using an inexpensive color sensor for rapid assessment of soil organic carbon. Geoderma 286, 98–103. <https://doi.org/10.1016/j.geoderma.2016.10.027>.
- Swetha, R.K., Dasgupta, S., Chakraborty, S., Li, B., Weindorf, D.C., Mancini, M., Silva, S. H.G., Ribeiro, B.T., Curi, N., Ray, D.P., 2022. Using NiX color sensor and Munsell soil color variables to classify contrasting soil types and predict soil organic carbon in Eastern India. Comput. Electron. Agric. 199, 107192 <https://doi.org/10.1016/j.compag.2022.107192>.
- Wasson, A.P., Rebetzke, G.J., Kirkegaard, J.A., Christopher, J., Richards, R.A., Watt, M., 2014. Soil coring at multiple field environments can directly quantify variation in

- deep root traits to select wheat genotypes for breeding. *J. Exp. Bot.* 65 (21), 6231–6249. <https://doi.org/10.1093/jxb/eru250>.
- Weindorf, D.C., Chakraborty, S., 2020. Portable X-ray fluorescence spectrometry analysis of soils. *Soil Sci. Soc. Am. J.* 84 (5), 1384–1392. <https://doi.org/10.1002/saj2.20151>.
- Weindorf, D.C., Zhu, Y., McDaniel, P., Valerio, M., Lynn, L., Michaelson, G., Clark, M., Ping, C.L., 2012a. Characterizing soils via portable X-ray fluorescence spectrometer. 2. Spodic and Albic Horizons. *Geoderma* 189–190, 268–277. <https://doi.org/10.1016/j.geoderma.2012.06.034>.
- Weindorf, D.C., Zhu, Y., Haggard, B., Lofton, J., Chakraborty, S., Bakr, N., Zhang, W., Weindorf, W.C., Legoria, M., 2012b. Enhanced pedon horizonation using portable X-ray fluorescence spectroscopy. *Soil Sci. Soc. Am. J.* 76 (2), 522–531. <https://doi.org/10.2136/sssaj2011.0174>.
- Weindorf, D.C., Paulette, L., Man, T., 2013. In-situ assessment of metal contamination via portable X-ray fluorescence spectrometry: Zlatna, Romania. *Environ. Pollut.* 182, 92–100. <https://doi.org/10.1016/j.envpol.2013.07.008>.
- Xu, P., Sun, C.X., Ye, X.Z., Xiao, W.D., Zhang, Q., Wang, Q., 2016. The effect of biochar and crop straws on heavy metal bioavailability and plant accumulation in a Cd and Pb polluted soil. *Ecotoxicol. Environ. Saf.* 132, 94–100. <https://doi.org/10.1016/j.ecoenv.2016.05.031>.
- Xu, S., Zhao, Y., Wang, M., Shi, X., 2018. Comparison of multivariate methods for estimating selected soil properties from intact soil cores of paddy fields by Vis-NIR spectroscopy. *Geoderma* 310, 29–43. <https://doi.org/10.1016/j.geoderma.2017.09.013>.
- Zhu, Y., Weindorf, D.C., Zhang, W., 2011. Characterizing soils using a portable X-ray fluorescence spectrometer. 1. Soil Texture. *Geoderma* 167, 167–177. <https://doi.org/10.1016/j.geoderma.2011.08.010>.
- Zhuang, P., Zou, B., Li, N.Y., Li, Z.A., 2009. Heavy metal contamination in soils and food crops around Dabaoshan Mine in Guangdong, China; implication for human health. *Environ. Geochem. Health* 31 (6), 707–715. <https://doi.org/10.1007/s10653-009-9248-3>.